WIND TUNNEL AND NUMERICAL EXPERIMENTS OF TWO-DIMENSIONAL STRATIFIED AIRFLOW OVER A HEATED ISLAND[Δ]

by

Robert N. Meroney*
Tetsuji Yamada**

Submitted for presentation at

1971 Winter Annual Meeting of

ASME

November 28 - December 2, 1971

Washington, D. C.

Δ Research Support Under THEMIS, Office of Naval Research, Contract No. N00014-68-A-0493-0001, Project No. NR062-414/6-6-68 (Code 438) is gratefully acknowledged.

* Associate Professor, Fluid Mechanics Program, Colorado State University, Fort Collins. Member ASME

** Research Associate, Colorado State University, Fort Collins

WIND TUNNEL AND NUMERICAL EXPERIMENTS OF TWO-DIMENSIONAL STRATIFIED AIRFLOW OVER A HEATED ISLAND

by

Robert N. Meroney and Tetsuji Yamada

Perturbations of a stratified shear flow by a heated boundary which may represent a heated island or an urban region, are investigated both experimentally and numerically. These experiments are apparently the first attempt to simulate the urban heat island effect in a wind tunnel facility. A numerical model was constructed to augment the wind tunnel results by solving a set of two dimensional, time dependent, and non-linear governing equations.

The results obtained by both methods agree quantitatively. The modifications of meteorological factors by urbanization, a downward wind and acceleration of a horizontal velocity in the surface layer over the upper half of a city, temperature cross-over, and frequent elevated inversion but less frequent surface inversion over the city during the night, are all reproduced.

A detailed examination of the results revealed a strong non-linearity which does not allow one to utilize conventional linearization techniques as a first approximation to the phenomenon.

Introduction:

Some of the most dramatic atmospheric phenomena occur as a result of sudden changes in the earth's surface temperature. In fact the driving mechanisms for the atmospheric circulation can be visualized as a complex extension on the global scale of the cellular motions of Benard's problem. On the smaller mesoscale the vagrancies of sea-land breezes, the effects of inversions on pollution in cities, or the flow over a heated island or a city represent examples of two and three dimensional interaction of a thermal boundary with the lower atmospheric shear flow. Specifically, the interaction of a metropolitan area as a heat source of finite extent on wind patterns and the potential penetration of heat plumes through inversion layers resulting in fumigation are relevant research topics which have received little or no attention. It has been postulated that recent convection motions and diffusion patterns encountered in the extensive study of Ft. Wayne, Indiana (Hilst and Browne, 1966) may be a result of the heat island phenomena.

The response of a two-dimensional turbulent boundary layer to abrupt changes in surface conditions has received extensive recent attention (Townsend, 1965a, 1965b; Chanda, 1958; Meroney and Cermak, 1967). The growth of the inner boundary layer due to a step change in roughness or temperature has been studied with respect to the sea-land breeze, evaporation, forest and agricultural crop meteorology, and for wind break design, (Cermak and Koloseus, 1953; Plate, 1964). The implications of the effects of finite non-homogeneous temperature distribution on the atmospheric boundary layer have not received such attention, and they shall be examined here numerically and by laboratory simulation.

The climate over cities is quite different from that over the surrounding rural area. Measurements of diurnal variation of temperature in Vienna, Austria (Mitchell 1962) and that in Frankfurt, Germany (Georgii 1968) are available. The urban station remained warmer most of the time ("urban heat island"). The largest temperature differences were observed at night both in summer and in winter. Maximum and minimum temperature in the cities occurred one or two hours after those in the suburbs. Many other climatic elements such as wind, radiation, humidity, cloudiness, and pollution are also changed by urbanization. Landsberg (1968) organized such climatic data into a table (see Table 1) to provide a quick understanding of average differences in climatic factors of urban and nonurban regions.

That certain cities have warmer temperature than their surroundings has been known since as early as the beginning of the eighteenth century, "but it was not until the relationships between the cities' heat island and the pathogenic and pernicious effects of air pollution were made evident that the study of this urban phenomenan was stimulated and accelerated" (Kopec 1970 p. 602). A comprehensive review of recent works on the matter are available in Peterson (1969) and in a W.M.O. technical note (1968).

Since urban heat island effects are most pronounced at night almost all past observers described the nocturnal heat island. Daytime temperature differences have also been observed (Ludwig and Kealoha, 1968; Preston-Whyte, 1970), but their magnitudes are generally small. Furthermore, measurements difficulties arise since (Kopec 1970); "daytime attempts to record temperature patterns were frustrated by constant sun-shade changes along the roads traveled, caused by trees, buildings and other roadside obstructions".

Most prominent field experiments were conducted by Duckworth and Sandberg (1954), DeMarrais (1961), Bornstein (1968), and Ludwig and Kealoha (1968). They examined wind and temperature fields over San Fransisco, California; Louisville, Kentucky; New York, N.Y.; and Dallas, Texas, respectively. Commonly observed heat island characteristics are listed as follows:

1. Very regular variation of daily temperature over flat unpopulated areas, whereas no generalizations of variation are obtained over urban region;
2. Less frequent occurrence of nocturnal inversion over a city;
3. One or more elevated inversion layers are formed over cities, whereas less frequently over rural regions;
4. Stronger nocturnal urban heat islands are observed in a calm, clear atmosphere;
5. Day time urban heat islands are less intense than the night counterpart;
6. Intensity of urban heat islands depends on meteorological (wind, stability) and physical (city size) factors;
7. Formation of "cross over" phenomena over cities;
8. Displacement of heat island center windward and
9. Upper limit of a direct effect of urban heat islands extends occasionally up to 1000 m but average height ranges 50 ~400 m.

Only a few attempts are recorded which try to quantitatively explain the phenomena above (Myrup 1969; Tag 1969; Olfe and Lee 1971; Vukovich 1971) However, similar phenomena to that of urban heat islands have been observed in oceanographic fields. Malkus and Bunker (1952) observed periodically-spaced rows of small cumuli leeward of small islands on sunny summer days. This phenomenon is now known as a "heated island" phenomenon (Malkus and Stern 1953). Wavy air motion at the lee side of an island in a strongly stably stratified airflow is the result

of unbalanced buoyancy forces as a result of the temperature difference between the island and over the surrounding ocean. This is a "lee wave" phenomenon as described previously by other authors, Malkus and Stern (1953), who noted the similarity between the heated island convection and airflow over a physical mountain. The heated island was replaced by an "equivalent mountain" whose shape is a function of the temperature excess of the island over the ocean, stability of the air, wind speed, and eddy diffusivity. The reliability of such a linear theory shall be examined by comparison with the data presented here.

Laboratory Model:

Geometric and dynamic similitude with matched boundary conditions must be satisfied to reproduce prototype atmospheric phenomena by model experiments (Cermak et al., 1966). It is extremely difficult to satisfy all similitude requirements simultaneously in the laboratory.

According to a linearized theory proposed by Stern and Malkus (1953) it is necessary to satisfy $\frac{\sqrt{gs}\ k}{U^2} > \frac{1}{2}$ in order to simulate an equivalent mountain capable of developing strong gravity waves downwind of a heated boundary. It will be easily seen that the above relation cannot be satisfied in any existing wind tunnel facility because it requires an unusually large stability and small velocity. For example, for similarity with $s = 3 \times 10^{-3}\ cm^{-1}$ $(\frac{\partial T}{\partial z} \approx 1^{o}C)$ and $k = 0.2\ cm^2/sec$ requires $u < 0.83$ cm/sec . If $u = 4$ cm/sec and $k = 0.2\ cm^2/sec$ then a $s > 1.63\ cm^{-1}$ is required for a simulation which is equivalent to $500^{o}C/cm$. Thus it is impossible to satisfy the relation $\sqrt{gs}\ k/U^2 > \frac{1}{2}$ unless viscosity k is artificially modified by a factor of at least 30. Hence, a thermal equivalent mountain in a wind tunnel experiment must take a plateau shape:

The mountain starts at the leading edge of the island and increases asymptotically to reach its maximum height directly above the end of the island, then decreases exponentially.

To see the shape of a thermal mountain which might be simulated the following numerical values are substituted into the same equation

$$u = 4 \text{ cm/sec},$$
$$s = 4.67 \times 10^{-3} \text{ cm}^{-1} \left(\frac{\partial T}{\partial z} = 1.4^{\circ}\text{C/cm}, \quad \bar{T} = 300 \text{ k}\right).$$

Molecular viscosity of 0.2 cm^2/sec, an island width of 8 cm, and a temperature excess over the island of 56°C were assumed. The computed mountain increased its height almost linearly to 8.4 cm at the end of the island then decreased exponentially taking the values of 6.1, 2.3, and 0.1 cm at $x = 30$, 100, and 350 cm, respectively.

Summarizing it evidently is necessary to obtain a velocity ranging between 4 to 15 cm/sec, and a temperature gradient of 0.5°C/cm to $1/5^{\circ}$C/cm to simulate atmospheric lee wave phenomena and heated island problems in a wind tunnel facility. The above requirements are equivalent to attaining a Froude number based on the wind tunnel height (60 cm) from 0.030 to 0.196. Although there are quite a few low speed, small wind tunnels (see Pope and Hooper, 1966 for general information) guidance for the design of a thermal wind tunnel is limited. Several reports are available, for example Plate and Cermak (1963), Strom and Kaplin (1968), Charpentier (1967), Scotti (1969), and Hewett et al.(1970). Since these facilities were designed to satisfy special purposes, duplication of their designs was not desirable. The tunnels of Strom and Kaplin, and Charpentier could not produce the strong temperature gradient required here; Scotti was primarily interested in a free shear layer whose thickness was about 1/4 inch and Hewett treated

flows whose duct Froude numbers were greater than $\frac{1}{\pi}$. Hence a facility has been designed to meet the needs outlined above.

Dimensions of the test section of the wind tunnel are 2 ft height x 2 ft width x 15 ft length (see Fig. 1.).

To provide a conditioned stratification in the test section, a series of heaters and cooling plates were added to the entrance, ceiling and floor of the tunnel. Sixteen electric heaters 6 x 24 in were arranged in a grid across the entrance section. Four larger heaters 2 x 3 ft were adhered to the adjustable ceiling. The floor was constructed from a series of water cooled aluminum ducts. Final tunnel provided thermal gradients as large as 1.25^{o}C/cm and wind speeds from 5 cm/sec to 200 cm/sec.

Copper-constantan thermocouples of 30 gage were utilized to monitor temperature variations. Sixteen thermocouples were mounted on the entrance heaters, four were on the ceiling heaters, and three were along the floor. Nine thermocouples mounted on a rake were used for vertical temperature distribution measurements.

A smoke wire method has been utilized to investigate flow field during thermal stratification. It has been perfected for a practical use at Engineering Research Center, Colorado State University. Figure 2. shows a smoke wire with attached instruments for velocity measurements. The advantage of the smoke wire method is an instantaneous visualization of the velocity profile.

There was no evidence to indicate a strong wave motion in the wind tunnel as found in other thermal wind tunnels. Temperature distributions just downstream of the entrance heaters, however, indicated that there existed strong disturbances in the airflow generated by large temperature differences between the heaters and the ambient

stream. These disturbances fortunately diminished rapidly in the streamwise direction, and no significant variations were experienced after 80 cm from the entrance heaters.

Numerical Model:

Ideally, numerical simulation can avoid all the difficulties encountered in a laboratory experiment. Since the former is a direct one to one simulation there is no need to consider scaling effects. The accuracy of a numerical experiment, however, depends on many factors, such as the particular differencing scheme used, the magnitude of grid and time increments, the boundary conditions imposed, the size of the computational area, etc. Therefore it is necessary to investigate the reliability of numerical results by other means. If the problem is simple enough a comparison with a known analytical solution might be possible. This is not normally the case, however, for such nonlinear problems as are described herein. A wind tunnel is a powerful candidate for this purpose. Once confidence is established in numerical procedures through a wind tunnel simulation, then the direct application of the numerical program to the atmosphere is reasonable. Another advantage to a numerical approach is that it is possible to extend or change meteorological variables easily. For example the effect of varying viscosity in a wind tunnel experiment may be examined by a numerical experiment. In this manner, theory, laboratory, and numerical simulation improve the understanding of complicated fluid motions.

The following set of equations (1), (2), and (3) together with the definition of the stream function (4) are to be integrated numerically with appropriate boundary and initial conditions.

$$\frac{D\zeta}{Dt} = K\nabla^2\zeta + \frac{g}{T}\frac{\partial T}{\partial x} \tag{1}$$

$$\zeta = \nabla^2\psi \tag{2}$$

$$\frac{DT}{Dt} = K'\nabla^2 T \tag{3}$$

$$u = -\frac{\partial\psi}{\partial z} \quad \text{and} \quad w = \frac{\partial\psi}{\partial x} \tag{4}$$

The assumptions inherent in this particular set of equations are discussed in detail by Yamada and Meroney (1971). As a result of a variety of test calculations the boundary conditions and grid for numerical integration were specified as shown in Fig. 3.

The primary difficulty associated with the approximation of a partial differential equation by a finite difference equation is due to the existence of nonlinear inertial terms such as $u\frac{\partial\zeta}{\partial x}$ or $w\frac{\partial\zeta}{\partial z}$ If one used a forward difference for a time derivative and a central difference for a space derivative then the difference equation for a differential equation $\partial\zeta/\partial t + u\,\partial\zeta/\partial x = 0$ is unconditionally unstable. (Richtmeyer and Horton, 1967). Hence no matter how small a time step is chosen small errors introduced in the computation grow without limit.

A solution to this instability has been provided by a "forward-backward" molecule which replaces convection terms by

$$\left(u\frac{\partial\zeta}{\partial x}\right)^n_{j,\ell} = u^n_{j,\ell}\,\frac{\zeta^n_{j,\ell} - \zeta^n_{j-1,\ell}}{\delta x} \quad \text{when} \quad u^n_{j,\ell} \geq 0$$

$$= u^n_{j,\ell}\,\frac{\zeta^n_{j+1,\ell} - \zeta^n_{j,\ell}}{\delta x} \quad \text{when} \quad u^n_{j,\ell} < 0$$

This relation states that when velocity $u^n_{j,\ell}$ is positive then the space derivative is approximated by a backward difference and when is negative then a forward difference is used. In this way the direction

of the convection is always the same as that of the local velocity components. All variables are transported from the upstream side of the point in a local sense. Subscript j and ℓ are j^{th} and ℓ^{th} grid points in x and z direction, respectively. In the same manner superscript n stands for n^{th} time step of integration. $n = 1$ is an initial time.

The upstream difference scheme has been used in many places, (for example, Estoque, 1961, 1962, 1968; Tonouye, 1966; Torrance and Rockett, 1969; Roache and Muller, 1970; Muller and O'Leary, 1970; etc.).

The upstream difference scheme may introduce an "unexpected" numerical damping which may under certain circumstances modify or control the solution for a given problem. The numerical result of this scheme is equivalent to added diffusion effect typified by a viscosity ν_p.

The term

$$\nu_p = \frac{|u|\delta x}{2}\left(1 - \frac{|u|\delta t}{\delta x}\right)$$

has been called the pseudo-viscosity or pseudo-diffusivity (Molenkamp, 1968). Molenkamp evaluated ν_p for typical thermal convection situations and numerical values were of the order of 35 $m^2 sec^{-1}$ which is comparative with typical measured turbulent viscosities ranging from 0 to 40 $m^2 sec^{-1}$.

The large damping effect introduced automatically in the upstream difference system is sometimes very convenient to filter or smooth out the computational errors developed near a large temperature discontinuity. They exist in the unstably stratified regions around a model heat island which magnifies even a small error introduced during computations. These perturbations usually do not represent physically

meaningful phenomena; therefore they should be numerically reduced or eliminated. Since the upstream finite difference expression itself has a smoothing character, any computational perturbations are smoothed out.

The sequence of operations involved in the numerical program and other details of boundary and initial conditions are found in Yamada & Meroney (1971).

Numerical integrations and experiments have been conducted in such a way that they may be directly compared. Therefore, it was convenient to use the same coordinate system in each case since a direct comparison of results was desirable. The wind tunnel test section is 50 cm height x 60 cm width x 450 cm length. Hence, about the same dimensional extent was utilized in the numerical computation (see Fig. 3). The area was divided by an 81 x 16 square mesh whose dimension is 4 x 4 cm. Therefore, a 60 cm height x 320 cm length area is the computational region — about the same size as the effective wind tunnel test section area.

Results and Discussion of Heated Island Effects

In a heated island phenomenon the surface temperature is a result of the total heat energy balance, including insulation, heat conduction into a soil layer or a building, convection and radiation to the atmosphere, etc. Since the above mechanism is complicated and not yet fully understood, it is convenient, in constructing a model, to specify *a priori* the surface temperature as a function of space and time. The daily change of the surface temperature is well described by a simple function such as a Fourier series with a small number of terms (Lönnquist, 1962). Since the purpose here was to simulate the basic

fluid phenomenon and not its time-dependent characteristics, a constant value for the temperature of the heated surface was selected in all cases.

Extensive temperature surveys in the wind tunnel were conducted to draw accurate isotherms over a heated area. A thermocouple-mounted rake was set along the centerline of the wind tunnel. Vertical measurements were made utilizing nine thermocouples of fixed heights, mounted on the rake.

Less extensive velocity measurements were obtained. The difficulty in measuring such small velocities in a temperature-stratified flow has already been described. The smoke-wire technique gave a very fast and clearly visible result in some regions. However, when the area of interest was located in turbulent flow regions (over the island, under the crest of lee waves, and close to the surface) smoke released from the heated wire dispersed rapidly due to the mixing effect of turbulence; hence the smoke trace on a picture was very poor. Therefore, construction of streamlines from a measured velocity field was not possible.

Flow visualization of streamlines using $TiCl_4$ streamers was attempted; however, results were only partial since, due to the very small basic wind speed, it was not possible to neglect the weight of the smoke.

Three heat islands were studied experimentally and numerically to investigate the effects of the intensity of heating at the island and of stability in the basic current. The Froude numbers shown in the figures are the averaged values of lower and upper regions. It is necessary to characterize the intensity of heating of different urban situations. It appears to be difficult to arrive at a parameter which does not contradict some prior usage or intuition. A non-homogeneity

parameter is proposed here whose variations will be discussed when laboratory and numerical results are obtained. One example will be given in section 5.3.4 to evaluate this parameter for a prototype observation of a heated island effect.

The non-homogeneity parameter introduced here is:

$$N_h = \frac{-\left(\frac{\partial T}{\partial z}\right)_{z=0}}{\frac{T_{island} - T_o}{L}} ,$$

where T_{island} and T_o are the temperature at the island and that of the surrounding surface, respectively. Temperature gradient over the island, $-\left(\frac{\partial T}{\partial z}\right)_{z=o}$, was taken from the experimental data at the center of the island. L is the width of a heated region. Additional information about flow conditions, such as basic wind speed, stability, wave length, viscosity, etc., are available in Table 2. Cases 1 and 2 had the same basic wind speed and stability (thus the same Froude number), but the intensity of heating varied (different N_h number). Case B-3 had a stronger stability but the same current of 6 cm/sec. Case B-3 also had the highest temperature excess of the three cases, but the N_h number was approximately the same magnitude as in Case B-1. Each numerical computation was conducted under the same flow conditions as in the corresponding experiment. The following sections describe the results of each case separately.

Case 1 — The Froude number was 0.100 which was averaged from values of 0.065 and 0.134 in the lower ($0 \leq z \leq 9$ cm) and upper ($z > 9$ cm), regions respectively. Isotherms of 295, 300, 302, 303, and 305^{o}K were drawn from the vertical temperature distribution at various locations. The result is shown in Fig. 4 together with

velocity profiles in the vicinity of the island. The equivalent thermal mountain shape was computed from the linear theory previously discussed. The height increased exponentially from 0 at $x = 0$ to the maximum height, 1.15 cm at the downward edge of the island ($x = 8$ cm). The height then decreased exponentially through the values of 1.14 cm, 1.05 cm, and 0.76 cm at $x = 15$, 50, and 200 cm respectively. The theoretical equivalent mountain had a very flat and broad structure more like a plateau than a step change mountain. Computation of the equivalent mountain height was based on the following initial conditions;

$\Delta T = 47.6^{\circ}K$,

$\overline{T} = 296.8^{\circ}K$,

$S_1 = 2.422 \times 10^{-3}$ cm^{-1} (stability in the lower region, $z \leq 8.9$ cm),

$U = 6$ cm/sec,

and

$K = 0.2$ cm^2/sec (kinematic viscosity).

The concept of the equivalent mountain can be applied only in the upper regions where the direct effect of heating from the island is negligible. In the present case it appears that the region is above $x = 15$ cm. The displacement of the $303^{\circ}K$ temperature contour line was about 8 cm. This is too large for the mountain height of 1.15 cm obtained theoretically from linear theory.

Existence of the basic current destroyed the symmetric thermal plume behavior which is seen in the field when there is no prevailing synoptic current (Delage and Taylor, 1971). The thermal plume over the island was swept streamward, and the isotherm structure was also displaced to the wind direction.

The velocity profiles at $x = 3$, 12 and 20 cm, as reduced from smoke wire photographs, are shown in the same figure (Fig. 4)

The profile at $x = 3$ cm indicates a strong surface wind accelerated by a counterclockwise sea breeze circulation at the windward edge of the island. This sea breeze motion introduced a strong negative velocity at the upper levels. Interaction with the basic current resulted in a weak negative flow as indicated in the figure. The surface currents on the lee side of the island were reversed; this indicates that the negative flow induced by the sea breeze circulation (generated by the temperature difference at the end portion of the heated island) was stronger than the basic wind. Further, the return currents of the sea breeze motion magnified the positive horizontal velocity component.

$TiCl_4$ smoke was introduced at the surface about 50 cm downwind from the heated plate (see the photograph in Fig. 4). Smoke was propagated backward against the basic current and rotated upward at the lee side of the island. Then the smoke trajectory separated into two directions - one traveled upstream and the other downstream. The flow directions are shown by arrows added to the picture. These coincide with temperature and velocity measurements discussed above.

A numerical simulation under equivalent flow conditions was conducted. The temperature of the island, however, was set at $320^{\circ}K$, whereas the laboratory measurement indicated $341^{\circ}K$. The justification for this variation is as follows. The laboratory model developed very strong temperature gradients in the surface region over the heated island, especially between the surface and the first point from the surface ($z = 0.635$ cm). This effect cannot be represented by the numerical model because minimum grid size is 4 cm. Therefore, an effective surface temperature was obtained by linearly extrapolating the first two values from the surface. Justification of this

boundary condition approximation depends, of course, on the comparison of the numerical results with the laboratory measurement.

The computed stream function,and the vorticity and temperature contour lines at $t = 27.11$ sec. are provided in Fig. 5. The streamline shows a closed region behind the island starting at the lee edge of the heated plate; this region corresponds to the shape of the equivalent thermal mountain. (This interpretation of the equivalent mountain from a separated streamline is one similar to that adopted in the field observation by Garstang et al. (1965), where a trajectory of a balloon released at the surface of the island was used to compute the thermal mountain height). Now we can see definite evidence of a thermal mountain induced by a heated island.

Its shape is broad as predicted by the linear theory, but the height is considerably higher (14 cm) than the theoretically predicted value (1.15 cm). In the theoretical evaluation of the thermal height, only the viscosity was an assumed value; the rest of the input values were obtained from the laboratory measurements. It has been mentioned that locally strong turbulent areas were observed over the heated island; thus, the turbulent mixing effect must be included in the numerical analysis.

Both the laboratory and the numerical heated island models predict rotation of the flow stream upward at the lee edge of the island and a maximum height at $x = 28$ cm, whereas the linearized theory for the heated island suggests that the equivalent mountain rises abruptly from the upstream edge of the island and the maximum height is attained at the lee edge of the island. Thus, the numerically computed mountain was displaced downstream. Vorticity contour lines indicate a pair of sea breeze circulations at both edges of the island. These cells are also convected downstream by the basic wind.

Experimental temperature distributions over and just leeward of the island show different characteristics from the rest of the locations: thermal profiles vary taking maximum and minimum values rather than monotonically increasing with height. Let us define the inversion haze as the point at which a minimum temperature first occurs. This haze height increases with distance x to 1.3, 2.4, 2.9, 5.0, 7.7, and 12.7 cm at x = 0, 2, 3, 6, 8, and 10 cm, respectively. These results explain part of the mechanism which creates "elevated inversions" observed over urban areas. In the prototype urban heat island phenomenon, a multi-leveled set of elevated inversion layers are observed. These additional layers may result from the radiation balance to urban pollutant haze.

Another interesting phenomenon observed in these measurements is a "thermal cross-over". The "cross-over" phenomenon occurs when temperatures at some height over a city take smaller values than those over the upstream rural area, i.e., there is a cooler region over the heated island before it matches with upstream temperature at some greater height.

Case 2 - To examine the effect of heating intensity upon the airflow, the surface temperature excess was increased to 84^{o}K. The equivalent mountain height predicted by the linear theory Eq. (2.2.2.7-2) was 2.02 cm, an increase of 76% over the previous case.

Figure 6 presents wind tunnel temperature and velocity measurements. General features are similar to the previous results shown in Fig. 5. In this case, however, the thermal plume penetrated more deeply into the basic current and larger variations of the isotherms were observed. The amplitude of the 306^{o}K contour line was about 14 cm, while the maximum variation of the previous case was 10 cm. Since the air over the heated island was displaced upward considerably, a

formation of cumulus clouds might be seen over its atmospheric equivalent if the air had enough moisture to condense. The cross over effect will be experienced traversing horizontally at height 30 cm from left to right in the figure. At first a high temperature is encountered until directly above the leading edge of the heated island. Next a cooler region exists up to about $x = 25$ cm or directly over the island; then a high temperature region again appears until the environment finally returns to the original temperature at $x = 60$ cm.

Velocity profiles in the same figure indicate a deeper sea breeze circulation than in Case 1. Over the island a strong wind with negative flow above it was again observed. Therefore the wind profile at this location had at least two maximums and one minimum. These were generated by the interactions of stratification of the air, sea breeze circulation induced by the heated plate, and the basic current. Negative flow downstream of the island extended about 20 cm upward and more than 60 cm horizontally.

A numerical simulation of the experiment was conducted with the same flow characteristics, except that the temperature at the island was $341^{\circ}K$ rather than the measured value of $377^{\circ}K$. The argument justifying this modification has already been mentioned in the discussion of the previous Case 1. Stream function, vorticity, and temperature contour lines at $t = 17.42$ sec are plotted in Fig. 7. A dividing streamline separated from the lee edge of the island, reached a maximum height of 28 cm at around $x = 40$ cm, and subsequently decreased its height gradually. Inside of this streamline was a closed region, which may correspond to an equivalent thermal mountain, whose height was again very large compared to the linear theory's predicted value of 2.02 cm.

Two large vorticities of opposite sign were again well developed over the island; both vorticities were bent streamward because of the basic current.

Both numerical and wind tunnel experiments simulated the effect of an introduction of an intense energy source. They reproduced the deep penetration of the heat plume, the large variation of isotherms, the intense development of a sea breeze circulation, the development of turbulent motion, and the complicated velocity profiles.

Case 3. In this case both stability and surface temperature were varied from the previous two cases in order to examine the effect of stability. The average Froude number was 0.064 as against 0.100. The same basic wind of 6 cm/sec was retained. Stronger stability effects are seen in Fig. 8 where measured isotherms and velocity profiles are plotted. Smaller penetration of the thermal plume in comparison with Case 2 was due to the much smaller Froude number in spite of the surface temperature increase to 412°K from 377°K. Case 3 (Fig. 8) displays a very similar isotherm pattern to that of Case 1 (Fig. 4) The counteraction of the more intense surface heating was a result of the more stable free stream retarding forces. This result underlines the necessity of using two different parameters to characterize the flow - one for the stability of the basic flow (Froude Number), and another to specify the heat island intensity (non-homogeneity parameter). The N_h numbers in Cases 1 and 3 were nearly equivalent; the Froude number in Case 3, however, is smaller than that in Case 1, resulting in less plume penetration. In fact, the scale of the sea breeze circulation in Case 3 is about 40% smaller than that in Case 1.

Numerical results are provided in Fig. 9 Estimated equivalent mountain height from a separated streamline was 24 cm, about ten times as large as the theoretically predicted value of 2.42 cm.

Comparison with prototype observations and other studies - Agreement of the results presented here with observational data (Stern and Malkus, 1953, Fig. 4, p. 111 and Fig. 6, p. 112; Fosberg, 1967, Fig. 2 on p. 893; Bornstein, 1968, Fig. 3, p. 578; Spelman, 1969, Fig. 9 on p. 116) is strikingly close. In each case the larger the Froude number and the larger the non-homogeneity parameter, the more deeply a heat plume penetrates into the atmosphere. There also exists an unstable region over the island, and isotherms display wavy configurations (see Fig. 6. The crest of an isotherm wave is always displaced streamward for larger Froude numbers and/or smaller N_h values (see Figs. 4 and 8 in the present results and Fig. 9 in Spelman (1969)).

Observational data include extremely small Froude number flows. Malkus' (1955) observations indicate that the largest Froude number was 0.06 for which a formation of cumulus cloud was observed. A very crude calculation was conducted to evaluate the N_h number, a heating intensity, for Malkus' observation. An island surface temperature excess of $1.5^{o}C$, an island width of 80 km, and a temperature gradient at the surface of $-0.3 \times 10^{-3}\ m^{-1}$ were utilized to obtain $N_h = 16$. In the present study, Case 3 has $Fr = 0.064$ and $N_h = 5.65$ which are approximately the same order of magnitude. Both results (Fig. 7 in Malkus and Fig. 8 in the present study) display many common features; however, the wave crests of the isotherms in the present study were displaced more streamward than those observed by Malkus. In the latter case a stronger blocking effect developed because of its larger N_h number.

LIST OF SYMBOLS

Symbol	Definition	Dimensions
$(Fr)_L$	Froude number, $\frac{U}{\sqrt{gs}\ L}$	-
$(\overline{Fr})_H$	Arithmetic averaged Froude number of those in lower and upper surface regions	-
g	Acceleration of gravity	LT^{-2}
H	A wind tunnel or a water channel height	L
j	j^{th} grid point in x direction in a finite difference expression	-
K	Total viscosity (kinematic viscosity plus eddy viscosity)	L^2T^{-1}
K'	Total diffusivity of heat	L^2T^{-1}
L	Characteristic length	L
ℓ	ℓ^{th} grid point in a finite-difference expression	L
n	n^{th} time step in a numerical computation	-
N_h	Non-homogeneity parameter to characterize a heating intensity of a heated island, $\frac{-(\frac{\partial T}{\partial z})_{z=0}}{\frac{T_{island} - T_o}{L}}$	
T	Temperature	θ
$\overline{T}$	Mean temperature	θ
T_{island}	Temperature over a heated island	θ
T_o	Surrounding surface temperature	θ
t	Time coordinate	T
$\overline{U}$	Mean longitudinal velocity component	LT^{-1}
u, v, w	Velocity components in x, y, and z direction, respectively	LT^{-1}

LIST OF SYMBOLS (Continued)

Symbol	Definition	Dimensions
x,y,z	Space coordinate in longitudinal, lateral, and vertical direction, respectively	L
δx, δz	Space grid increments in x and z directions respectively in a finite-difference expression	L
δt	Time grid increment in a finite-difference expression	T
ΔT	Temperature excess over a heated island, $T_{island} - T$.	θ
ζ	Vorticity component in y direction $\frac{\partial w}{\partial x} - \frac{\partial u}{\partial z}$	T^{-1}
ν_p	Pseudo-viscosity introduced in the upstream finite-difference approximation scheme	L^2T^{-1}
ψ	Stream function	L^2T^{-1}
1,2	Subscripts to indicate the quantities in a lower and an upper surface layer when different stabilities are used in the layers	-

Symbols used to indicate dimension are M - Mass, L - Length, T - Time, θ - Temperature

BIBLIOGRAPHY

Bornstein, R. D., 1968; "Observations of the Urban Heat Island Effect in New York City," J. Appl. Meteor., 7, pp. 575-582.

Cermak, J. E. and Koloseus, H. J., 1953; "Lake Hefner Model Studies of Wind Structure and Evaporation," Final Report Part I and II, Contract No. bsr-57053, Bureau of Physics, U.S. Navy, Colorado State University Report No. CER54JEC20.

Cermak, J. E., ed., 1966; "Simulation of Atmospheric Motion by Wind Tunnel Flows," Fluid Dynamics and Diffusion Lab., Colorado State University.

Chanda, Benoyendra, 1958; "Turbulent Boundary Layer over Heated and Unheated Plane, Rough Surfaces," Colorado State University Report CER58BC21, AFCRC TN-58-428.

Charpentier, C., 1967; "Etude de la Stabilité d'un Gradient Thermique Produit Artificiellement dans un Ecoulement à Basse Vitesse au Moyen d'une Grille d'Eléments Chauffants," Départment Méchanique Théorique, Electricite de France 6, Quai Watier-78 Chatou, 12 pp.

Delage, Y., and Taylor, P. A., 1970; "Numerical Studies of Heat Island Circulation," Boundary Layer Meteorology, 1, pp. 201-226.

DeMarrais, G. A., 1961; "Vertical Temperature Difference Observed over an Urban Area," Bull. Amer. Meteor. Soc., 42, No. 8, pp. 548-554.

Duckworth, F. S., and Sandberg, J. S., 1954; "The Effect of Cities upon Horizontal and Vertical Temperature Gradients," Bull. Amer. Meteor. Soc., 35, No. 5, pp. 198-207.

Estoque, M. A., 1961; "A Theoretical Investigation of the Sea Breeze," Q. J. Roy. Meteor. Soc., 87, pp. 136-346.

Estoque, M. A., 1962; "The Sea Breeze as a Function of the Prevailing Synoptic Situation," J. Atmosp. Science., 19, pp. 245-250.

Estoque, M. A. and Bhumralkar, C. M., 1968; "Theoretical Studies of the Atmospheric Boundary Layer," Final Rep., Grant DA-AMC-28-043-67-G2, Institute of Atmospheric Science, University of Miami, Coral Gables, Florida 33124.

Fosberg, M. A., 1967; "Numerical Analysis of Convective Motions over a Mountain Ridge," J. Appl. Met., 6, No. 5, pp. 889-904.

Fosberg, M. A., 1969; "Airflow over a Heated Coastal Mountain," J. Appl. Met., 8, No. 3, pp. 436-442.

Garstang, M, Boaz, W. J., and La Seur, N. E., 1965; "The Equivalent Heat Mountain, A Preliminary Study," Florida State University Department of Meteor., 26 pp.

Georgii, H. W., 1968; "The Effects of Air Pollution on Urban Climates," in Urban Climates, W.M.O. Tech. Note No. 108, pp. 214-237.

Hewett, T. A., Fay, J. A., and Hoult, D. P., 1970; "Laboratory Experiments of Smokestack Plumes in a Stable Atmosphere," Fluid Mechanics Laboratory, Department of Mechanical Engineering, Massachusetts Institute of Technology, 31 pp.

Hilst, G. R. and Bowne, N. E., 1966; "A Study of the Diffusion of Aerosols Released from Aerial Line Sources Upwind of an Urban Complex," Final Report, Project No. 4V025001A128, Hartford, Conn., The Travelers Research Center, Inc., Vol. I, and Vol. II.

Landsberg, H. E., 1956; "The Climate of Towns," in Man's Role in Changing the Face of the Earth, Chicago, Illinois, University of Chicago Press, pp. 584-606.

Landsberg, H. E., 1968, "Climates and Urban Planning," in Urban Climates, W.M.O. Tech. Note No. 108, pp. 364-374.

Lönnquist, O., 1962; "On the Diurnal Variation of Surface Temperature," Tellus, XIV, 1, pp. 96-101.

Ludwig, F. L. and Kealoha, J. H. S., 1968; "Urban Climatological Studies," Stanford Research Institute, Menlo Park, California.

Malkus, J. S. and Bunker, A. F., 1952; "Observational Studies of the Air Flow over Nantucket Island During the Summer of 1950,: Pap. Phys. Ocean. Meteor., Mass. Inst. Tech. and Woods Hole Ocean. Inst. 12, No. 2, 50 pp.

Malkus, J. S., and Stern, M. E., 1953; "The Flow of a Stable Atmosphere Over a Heated Island, Part I," J. Meteor., 10, pp. 30-41.

Malkus, J. S., 1955; "The Effects of a Large Island Upon the Trade-Wind Air Stream," Q. J. Roy. Meteor. Soc., 81, pp. 538-550.

Meroney, R. N. and Cermak, J. E., 1967; "Characteristics of Diffusion Within Model Crop Canopies," Symposium on the Theory and Measurement of Atmospheric Turbulence and Diffusion in the Planetary Boundary Layer, Albuquerque, December 5-7, 1967.

Mitchell, J. M., Jr., 1961; "The Temperature of Cities," Weatherwise, 14, pp. 224-229.

Molenkamp, C. R., 1968; "Accuracy of Finite-Difference Methods Applied to the Advection Equation," J. Appl. Meteor., 7, pp. 160-167.

Mueller, T. J., and O'Leary, R. A., 1970; "Physical and Numerical Experiments in Laminar Incompressible Separating and Reattaching Flows," AIAA 3rd Fluid and Plasma Dynamics Conference, Los Angeles, California, June 29- July 1, 1970, 15 pp.

Myrup, L. O.; 1969; "A Numerical Model of the Urban Heat Island," J. Appl. Meteor., 8, No. 6, pp. 908-918.

Olfe, D. B., and Lee, R. L., 1971; "Linearlized Calculations of Urban Heat Island Convection Effects," AIAA Paper No. 71-13, AIAA 9th Aerospace Sciences Meeting, New York, New York, 14 pp.

Peterson, J. T., 1969; "The Climate of Cities: A Survey of Recent Literature," U.S. Department of Health, Educ., and Welfare, Pub. Health Service, Consumer Protection and Environmental Health Service, Nat. Air Poll. Contr. Admin., Raleigh, North Carolina, 48 pp.

Plate, E. J., and Cermak, J. E., 1963; "Micrometeorological Wind Tunnel Facility, Description and Characteristics," Final Report on Contract No. DA36-039-SC-80371 with Meteorology Department, U.S. Army Electronic Research and Development Activity, Fort Huachuca, Arizona, Fluid Dynamics and Diffusion Laboratory, Colorado State University, Fort Collins, Colorado, CER63-EJP-JEC9, 39 pp.

Pope, A., and Hooper, J. J., 1966; Low-Speed Wind Tunnel Testing, John Wiley and Sons.

Preston-Whyte, R. A., 1970; "A Spatial Model of an Urban Heat Island," J. Appl. Meteor., 9, pp. 571-573.

Richtmyer, R. D. and Morton, K. W., 1967; Difference Methods for Initial-Value Problems, Interscience Publishers, New York, 405 pp.

Roache, P. J. and Muller, T. J., 1970; "Numerical Solutions of Laminar Separated Flows," AIAA J., 8, No. 3, pp. 530-538.

Scotti, R., 1969; "An Experimental Study of a Stratified Shear Layer," Rep. No. AS-69-1, Contract No. USCDE-22-129-68(G), College of Engineering, University of California, Berkeley, 154 pp.

Spelman, M. J., 1969; "Atmospheric Modification of Surface Influences, Pt. II. Response of the Atmosphere to the Surface Features of a Tropical Island," Rep. No. 15, Department of Meteorology, The Pennsylvania State University, University Park, Pennsylvania, pp. 73-132.

Stern, M., 1955; "Theory of the Mean Atmospheric Perturbations Produced by Differential Surface Heating," J. of Met., 11, pp. 495-502.

Strom, G. H., and Kaplin, E. J., 1968; "Final Report Convective Turbulence Wind Tunnel Project," Rep. No. 504.04, New York University, School of Engineering and Science, University Heights, New York, New York 10453, 38 pp.

Tag, P. M., 1969; "Surface Temperatures in an Urban Environment," in Atmospheric Modification by Surface Influences, Department of Meteor., The Pennsylvania State University, University Park, Penn., 72 pp.

Tanouye, E. T., 1966; "The Response of the Atmosphere to a Localized Heat Source at the Earth's Surface," in Theoretical Studies of the Atmospheric Boundary Layer, Hawaii Institute of Geophysics, University of Hawaii, pp. 123-173.

Torrance, K. E., and Rocket, J. A., 1969; "Numerical Study of Natural Convection in an Enclosure with Localized Heating from Below - Creeping Flow to the Onset of Laminar Instability," J. Fluid Mech., 36, Part 1, pp. 33-54.

Townsend, A. A., 1965a; "Self-Preserving Flow Inside a Turbulent Boundary Layer," J. Fluid Mechanics, 22, pp. 773-797.

Townsend, A. A., 1965b; "The Response of a Turbulent Boundary Layer to Abrupt Changes in Surface Conditions," J. Fluid Mechanics, 22, pp. 799-822.

Vukovick, F. M., 1971; "A Theoretical Analysis of the Effect of Mean Wind and Stability on a Heat Island Circulation Characteristic of an Urban Complex," Month. Weather Review (to be published).

W.M.O. Tech. Note No. 108, 1968; "Urban Climates," Proceedings of the W.M.O. Symposium on Urban Climates and Building Climatology, Brussels, (Vol. I), 390 pp.

Yamada, T., and Meroney, R. N., 1971; "Numerical and Wind Tunnel Simulation of Stratified Shear Layers to Nonhomogeneous Surface Features," CER70-71TY-RNM62, Fluid Dynamics and Diffusion Laboratory, College of Engineering, Colorado State University, Fort Collins, Colorado.

TABLE 1

Average Change in Climatic Elements Caused by Urbanization (Landsberg, 1968)

Element	Comparison with rural environment
Contaminants:	
condensation nuclei and particulates;	10 times more
gaseous admixtures	5 to 25 times more
Cloudiness:	
cover;	5 to 10% more
fog, winter;	100% more
fog, summer	30% more
Precipitation:	
totals;	5 to 10% more
days with less than 5 mm;	10% more
snowfall	5% less
Relative humidity:	
winter;	2% less
summer	8% less
Radiation:	
global;	15 to 20% less
ultra-violet, winter;	30% less
ultra-violet, summer;	5% less
sunshine duration	5 to 15% less
Temperature:	
annual mean;	0.5 to 1.0°C more
winter minima (average);	1 to 2°C more
heating degree days	10% less
Wind speed:	
annual mean;	20 to 30% less
extreme gusts;	10 to 20% less
calms	5 to 20% more

TABLE 2

A Summary of Wind Tunnel and Numerical Studies

	EXPERIMENTAL										THEORETICAL (Linearlized)				NUMERICAL			
Variables / Case	Velocity U (cm/sec)	Stability S (cm^{-1})	$\frac{\partial T}{\partial Z}$ (^oC/cm)	Diffusivity K (cm^2/sec)	Temp. Excess δT (^oC)	Island Width 2D (cm)	Charac. Length L (cm)	$(\overline{Fr})_L$	$(Re)_L$	$(N_h)_{x=D}$	Amplitude $A=\frac{\Delta T}{\partial T/\partial Z}$ (cm)	Effective Height $M=A(1-\frac{1}{e})$ (cm)	x_o (cm)	$M_{X=2D}$ (cm)	Mmax (cm)	K (cm^2/sec)	ΔT (^oC)	$(N_h)_{x=D}$
Case 1	6.0	1.5×10^{-3} *(2.42,0.57)	0.45 (0.72,0.17)	0.2 (assumed)	48	8	60	0.100 (0.065,0.134)	1800	5.40	66	42	735	1.15	14	2.7	26	0.99
Case 2	6.0	1.5×10^{-3} (2.42,0.57)	0.45 (0.72,0.17)	0.2 (assumed)	84	8	60	0.100 (0.065,0.134)	1800	7.40	116	73	735	2.02	28	6.3	57	0.86
Case 3	6.0	3.05×10^{-3} (4.46,1.59)	0.95 (1.40,0.52)	0.2 (assumed)	107	8	60	0.064 (0.048,0.080)	1800	5.55	76	48	364	2.42	24	2.3	55	0.71

* The first number shows the value in the lower layer and the second one indicates the value in the upper layer

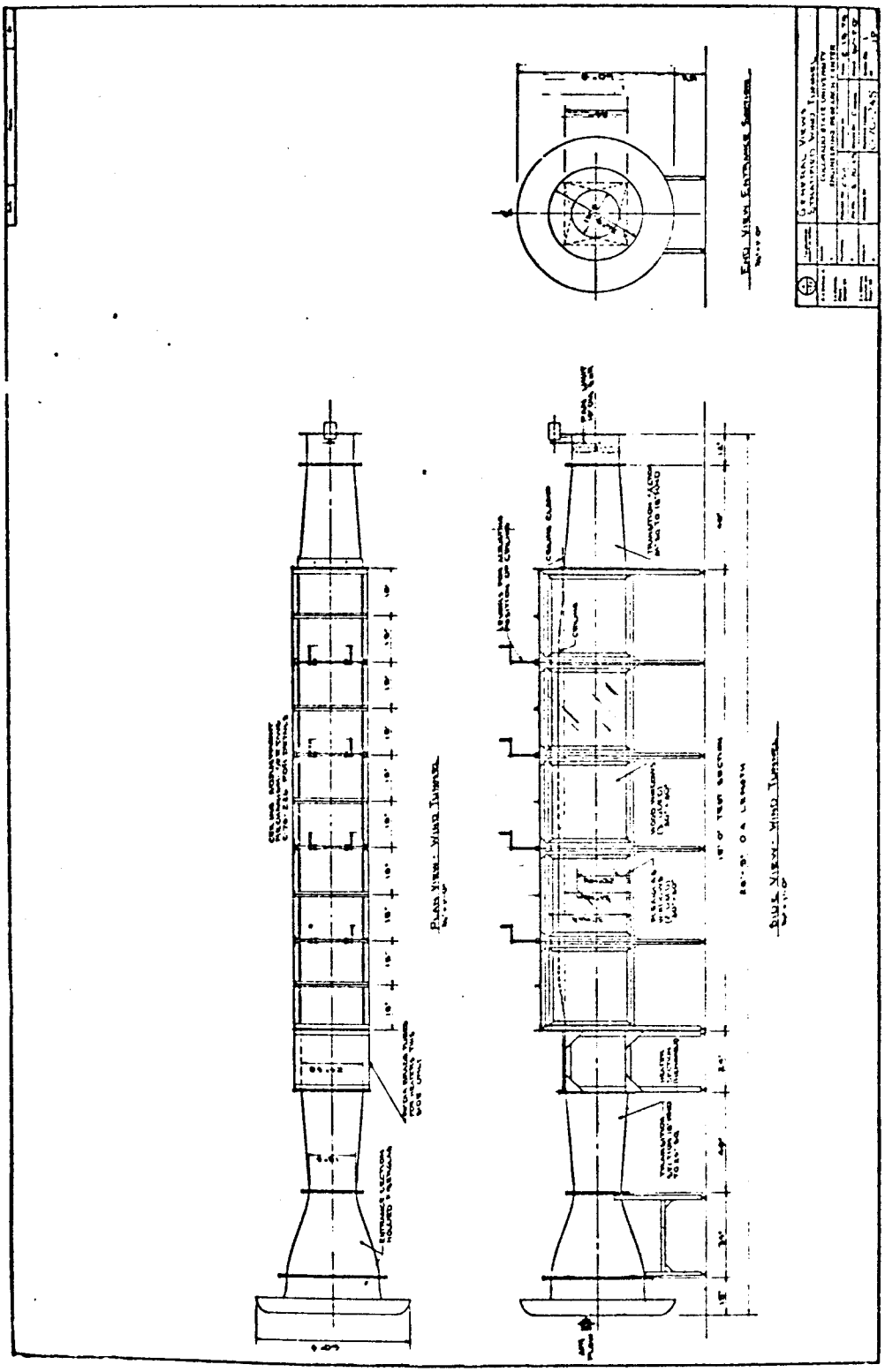

Fig. 1 General views of the stratified wind tunnel.

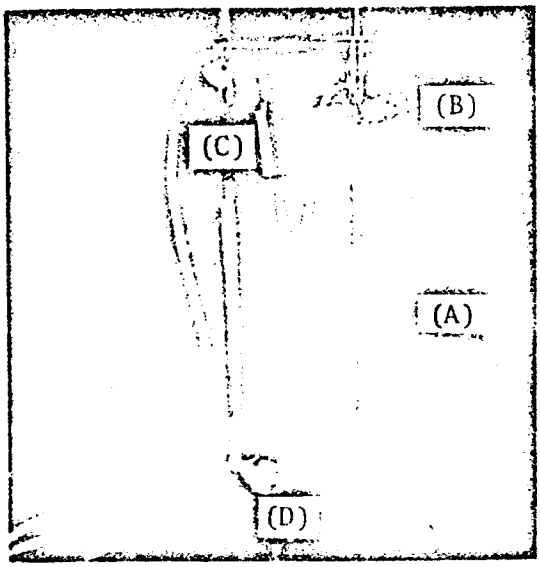

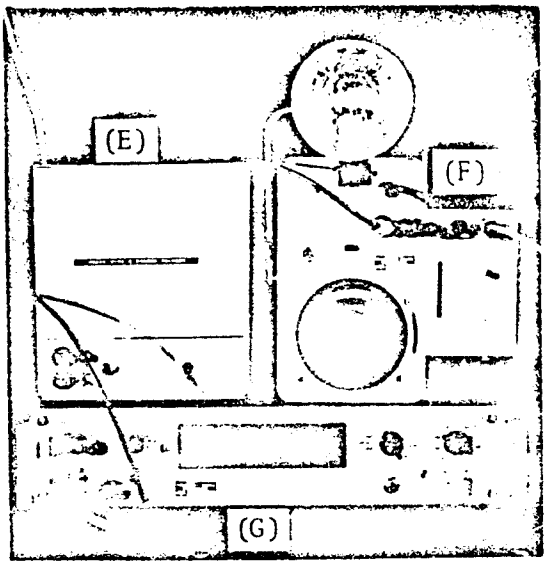

(A) Nichrome Wire

(B) Oil Outlet

(C) Oil Reservoir

(D) Air Bag

(E) Trigger Circuit

(F) Strobe System

(G) Electronic Counter

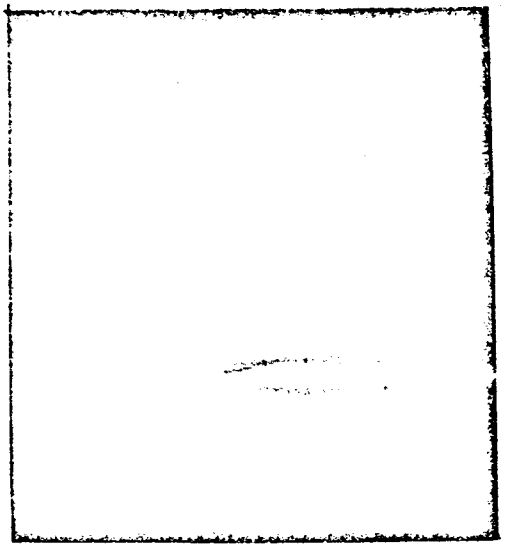

A Typical Velocity Profile (Neutral Case)

Fig. 2 Smoke wire and attached instruments for velocity measurements. A typical velocity profile is included.

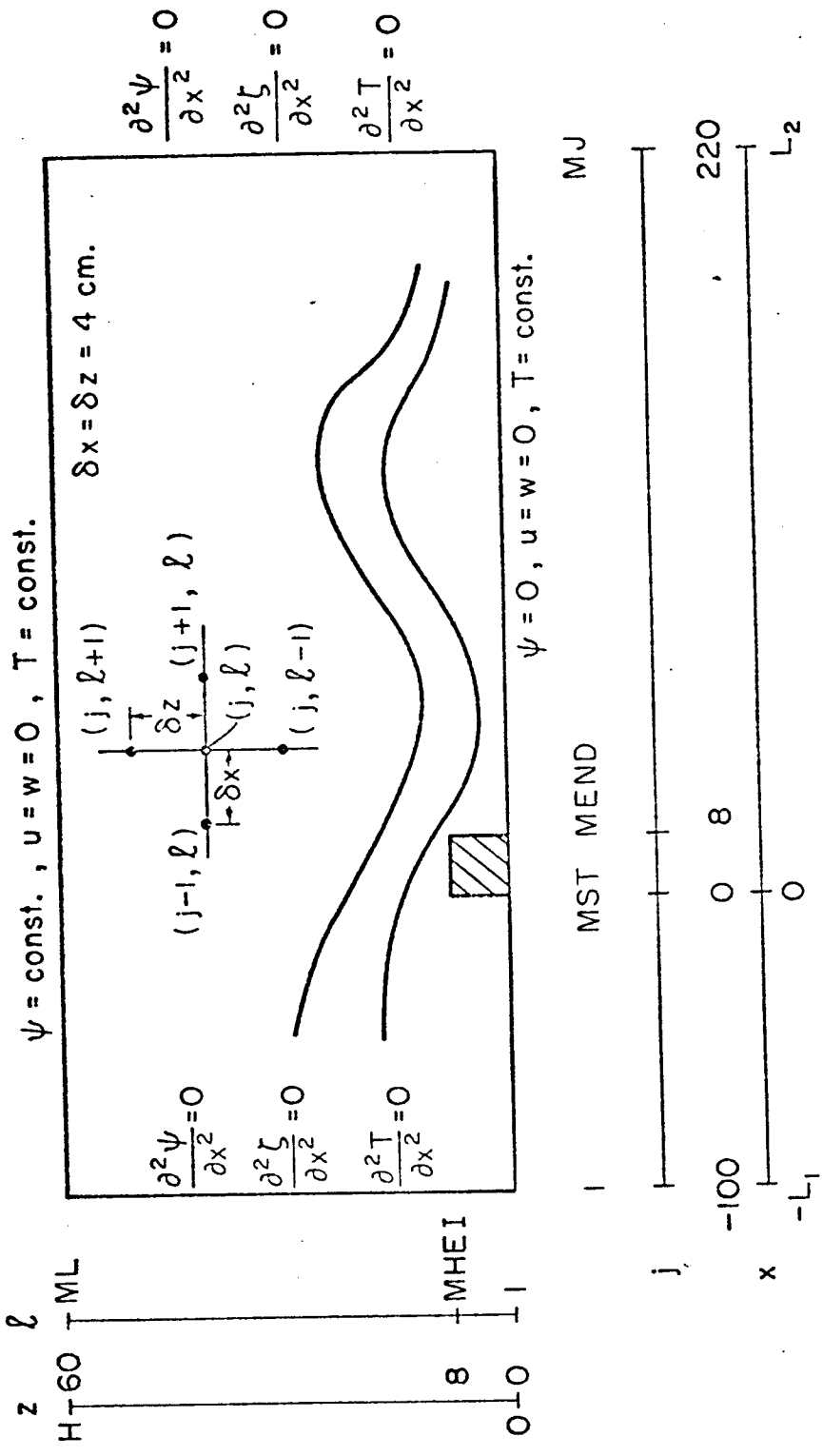

Fig. 3 Schematic diagram of the numerical computational region, the grid system, and boundary conditions.

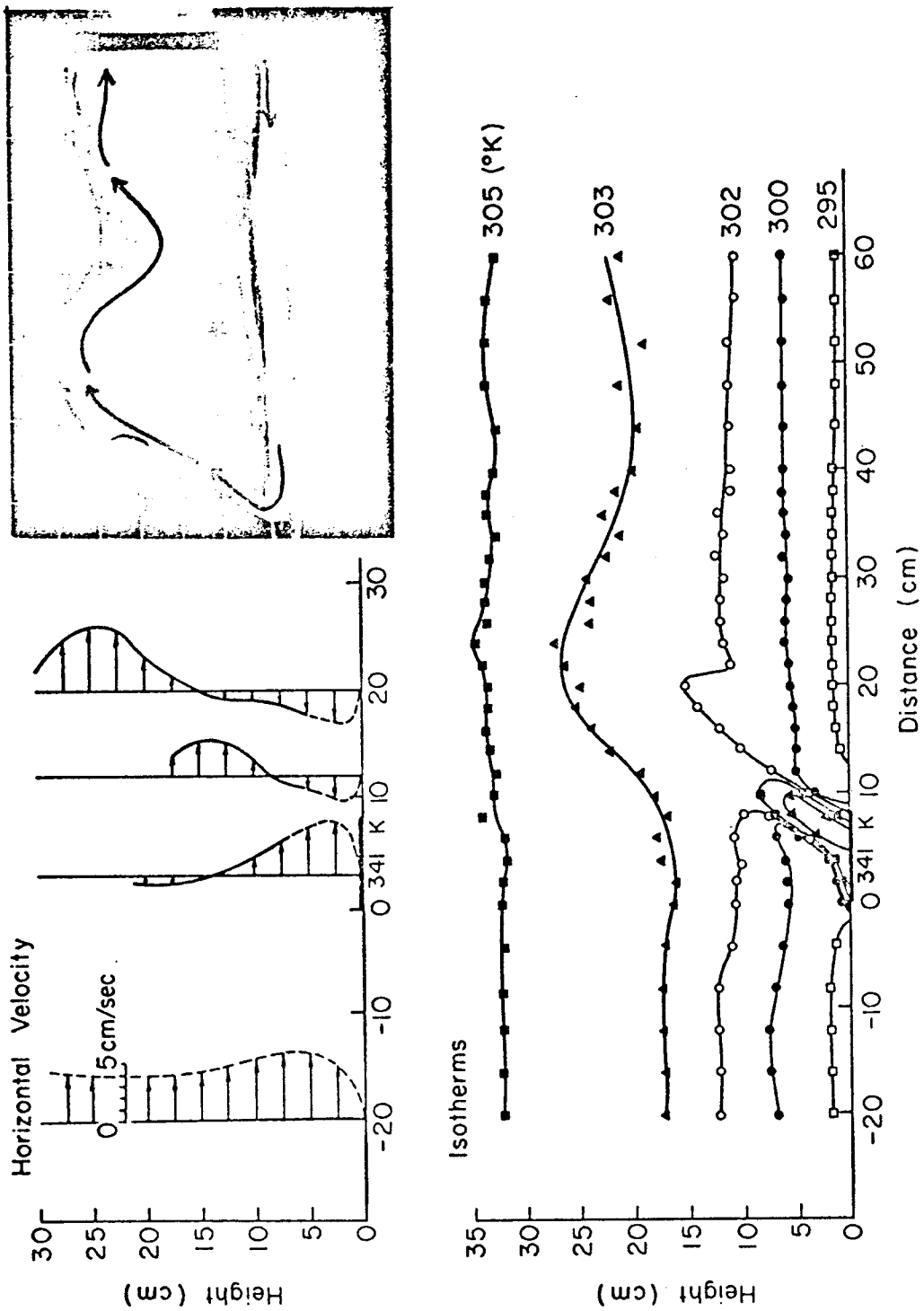

Fig. 4 Case 1 (Experimental): Measured horizontal velocity profiles and isotherms when $(Fr)_H = 0.100$, and $N_h = 5.40$. Photograph shows a flow visualization by $TiCl_4$ smoke introduced at the right bottom corner of the picture.

Stream Function

Vorticity

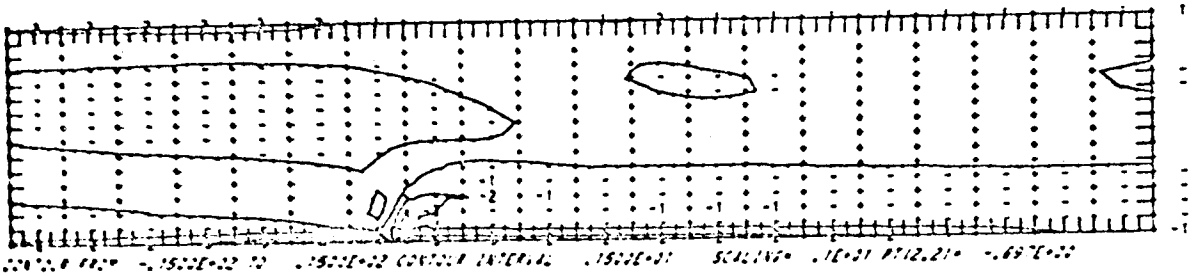

Temperature

Fig. 5 Case 1 (Numerical): Computed stream function, vorticity, and temperature contour lines at t = 27.11 sec. under the same flow conditions as in Fig. 4.

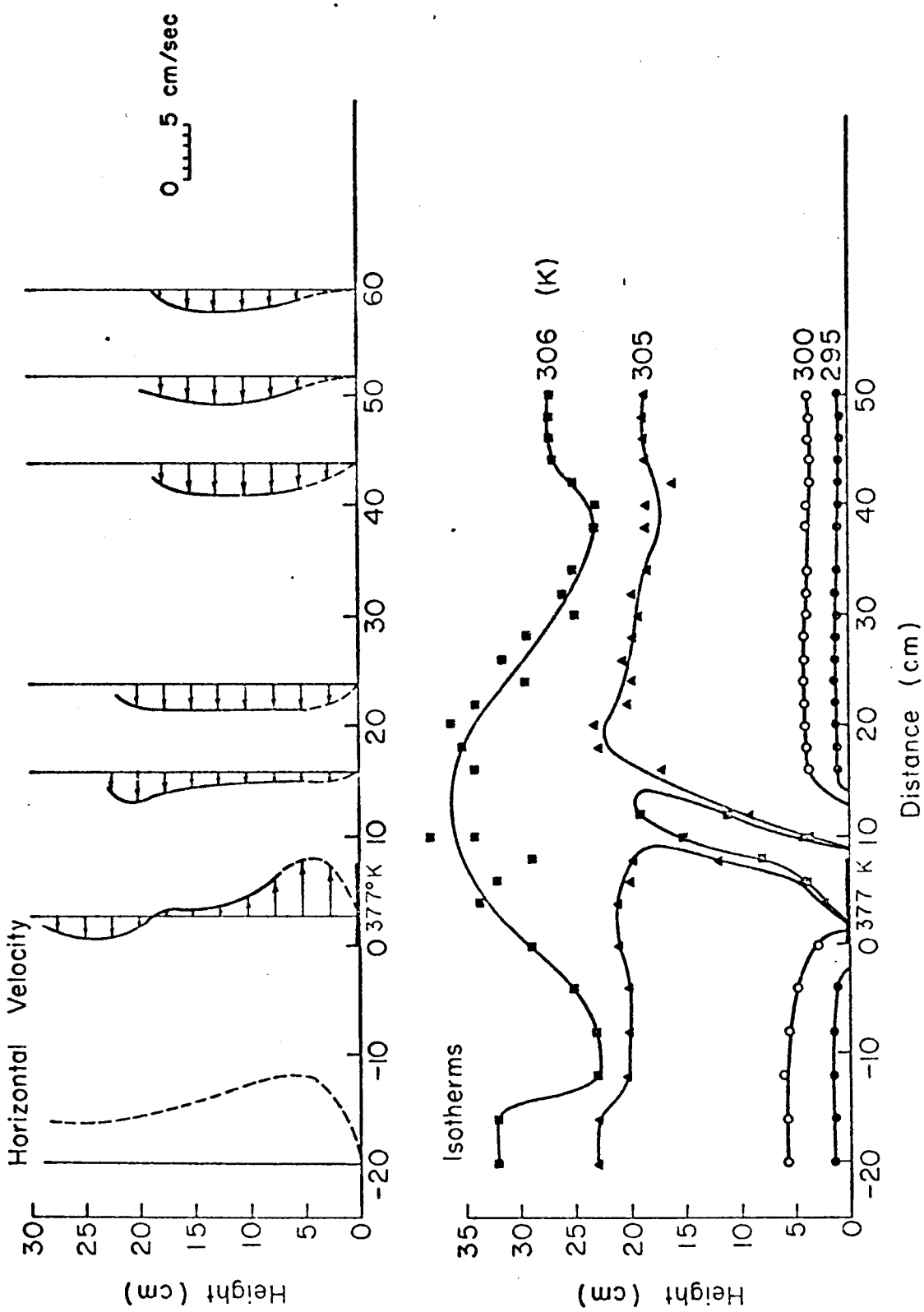

Fig. 6 Case 2 (Experimental): Measured horizontal velocity profiles and isotherms when $(Fr)_H = 0.100$, and $N_h = 7.40$.

Stream Function

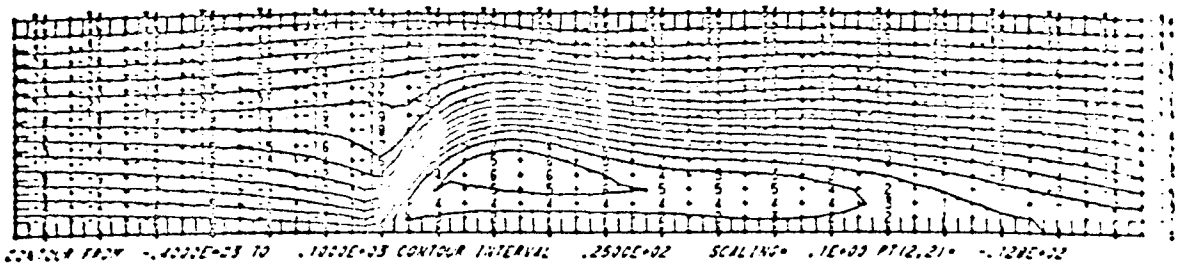

Vorticity

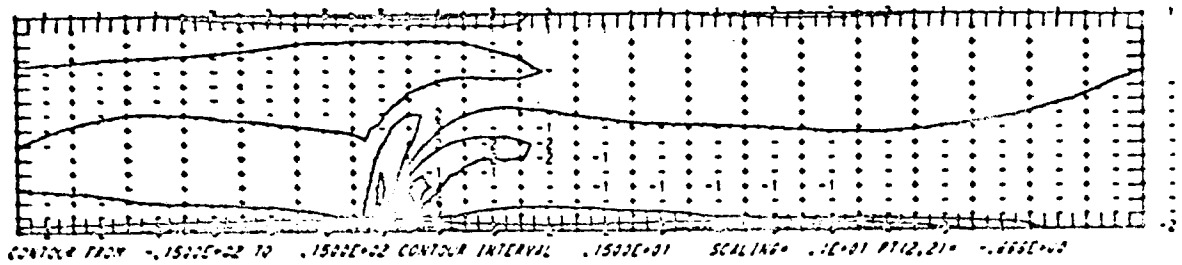

Temperature

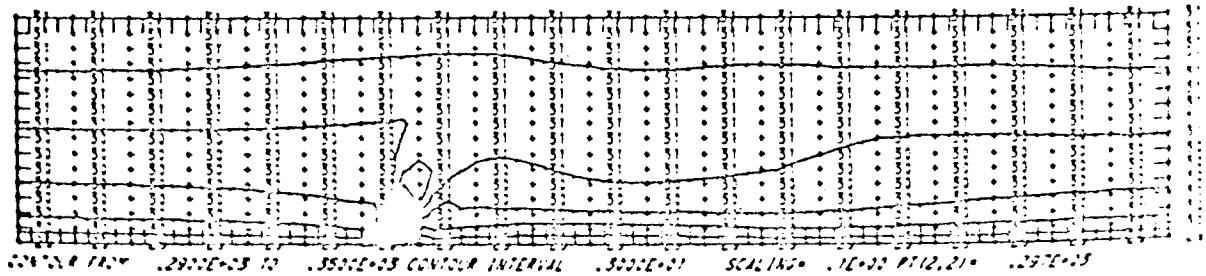

Fig. 7 Case 2 (Numerical): Computed stream function, vorticity and temperature contour lines at t = 17.42 sec. under the same flow conditions as in Fig. 6.

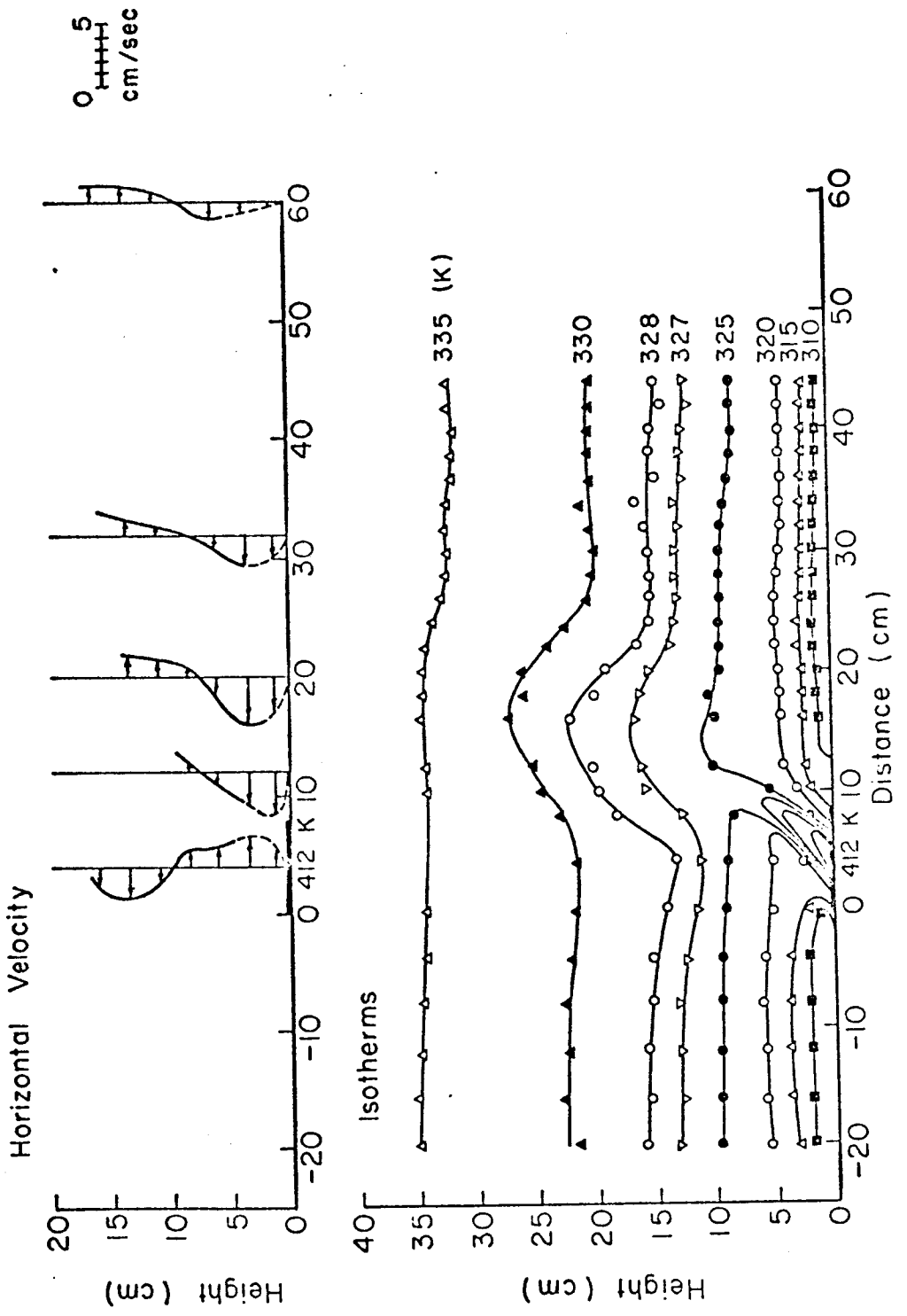

Fig. 8 Case 3 (Experimental): Measured horizontal velocity profiles and isotherms when $(\overline{Fr})_H = 0.064$, and $N_h = 5.55$.

Stream Function

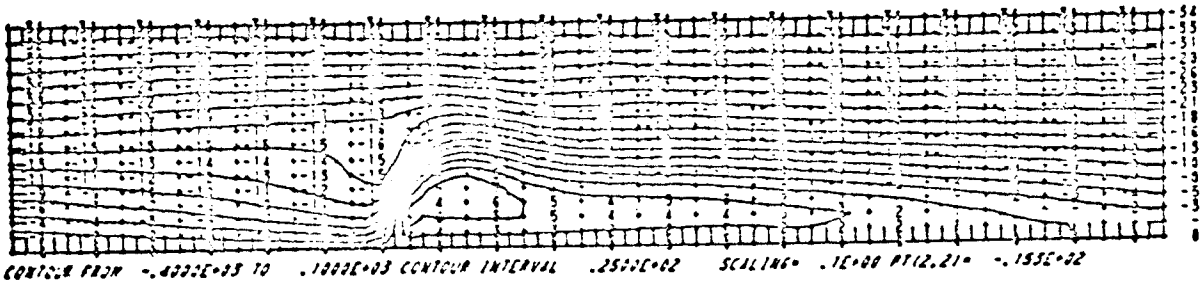

Vorticity

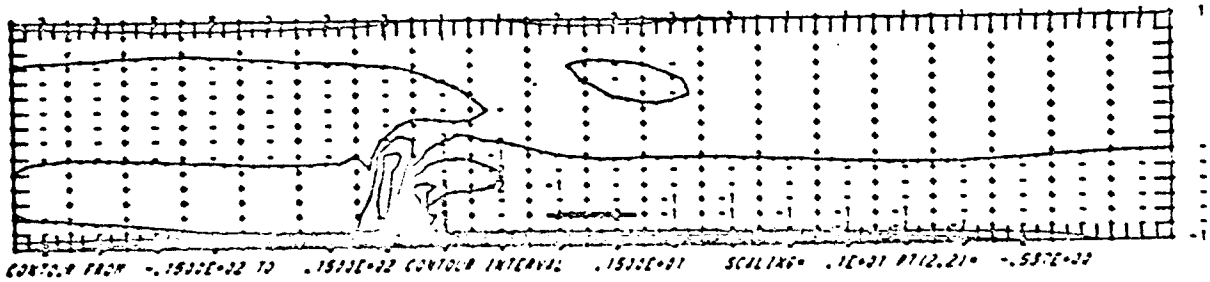

Temperature

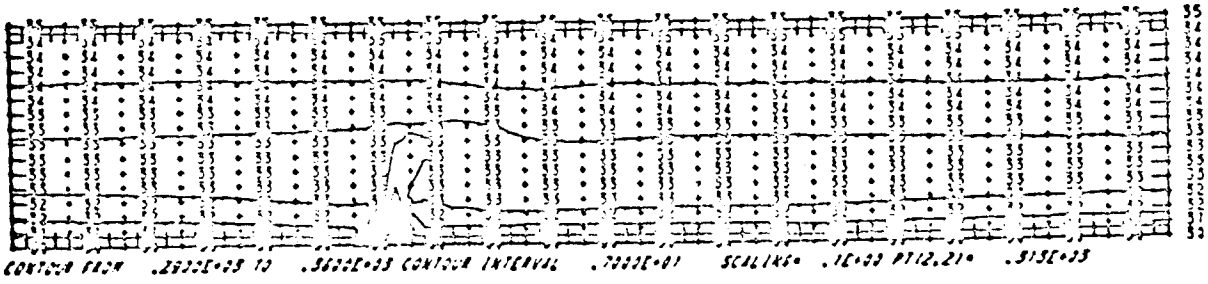

Fig. 9 Case 3 (Numerical): Computed stream function, vorticity, and temperature contour lines at t = 16.94 sec. under the same conditions as in Fig. 8.